

**Solid-State Structures**

# Tricyanidoferrates(–IV) and Ruthenates(–IV) with Non-Innocent Cyanido Ligands

Franziska Jach,\* Frank R. Wagner, Zeeshan H. Amber, Michael Rüsing, Jens Hunger, Yurii Prots, Martin Kaiser, Matej Bobnar, Anton Jesche, Lukas M. Eng, Michael Ruck, and Peter Höhn

Dedicated to Professor Wolfgang Kaim on the occasion of his 70<sup>th</sup> birthday.

**Abstract:** Exceptionally electron-rich, nearly trigonal-planar tricyanidometalate anions  $[\text{Fe}(\text{CN})_3]^{7-}$  and  $[\text{Ru}(\text{CN})_3]^{7-}$  were stabilized in  $\text{LiSr}_3[\text{Fe}(\text{CN})_3]$  and  $\text{AE}_{3.5}[\text{M}(\text{CN})_3]$  ( $\text{AE} = \text{Sr}, \text{Ba}$ ;  $\text{M} = \text{Fe}, \text{Ru}$ ). They are the first examples of group 8 elements with the oxidation state of –IV. Microcrystalline powders were obtained by a solid-state route, single crystals from alkali metal flux. While  $\text{LiSr}_3[\text{Fe}(\text{CN})_3]$  crystallizes in  $P6_3/m$ , the polar space group  $P6_3$  with three-fold cell volume for  $\text{AE}_{3.5}[\text{M}(\text{CN})_3]$  is confirmed by second harmonic generation. X-ray diffraction, IR and Raman spectroscopy reveal longer C–N distances (124–128 pm) and much lower stretching frequencies (1484–1634  $\text{cm}^{-1}$ ) than in classical cyanidometalates. Weak C–N bonds in combination with strong M–C  $\pi$ -bonding is a scheme also known for carbonylmetalates. Instead of the formal notation  $[\text{Fe}^{-\text{IV}}(\text{CN}^-)_3]^{7-}$ , quantum chemical calculations reveal non-innocent intermediate-valent  $\text{CN}^{1.67-}$  ligands and a closed-shell  $d^{10}$  configuration for Fe, that is,  $\text{Fe}^{2-}$ .

## Introduction

In 1706, synthetic chemistry of cyanidometalates started with the accidental discovery of Prussian blue,  $\text{Fe}_4[\text{Fe}(\text{CN})_6]_3$ , a pigment with many additional applications still in use today.<sup>[1]</sup> Classical cyanidometalates exhibit strong  $\sigma$ -donor bonds between  $\text{CN}^-$  ligand and transition metal cation, which allow relatively high positive metal oxidation states, for example, in  $[\text{Fe}^{\text{III}}(\text{CN})_6]^{3-}$ . Thus,  $\text{CN}^-$  is usually regarded as an innocent, redox-inactive ligand, and simple counting rules give a fairly realistic model of the electron distribution.<sup>[2]</sup> This is evident from C–N distances and stretching frequencies

How to cite: *Angew. Chem. Int. Ed.* **2021**, *60*, 15879–15885  
 International Edition: doi.org/10.1002/anie.202103268  
 German Edition: doi.org/10.1002/ange.202103268

$\nu(\text{CN})$ , which are in most cases similar for cyanido complexes (113–116 pm, 2000–2200  $\text{cm}^{-1}$ ) and simple salts such as NaCN (116 pm, 2080  $\text{cm}^{-1}$ ).<sup>[3]</sup>

In contrast, the previously reported electron-rich tricyanidocobaltate  $\text{Ba}_3[\text{Co}(\text{CN})_3]$  displays significantly longer C–N distances (123.5(5) pm) and much lower stretching frequencies (1680–1696  $\text{cm}^{-1}$ ), indicating a severe weakening of the C–N bonds.<sup>[4]</sup> Experimental and computational studies on  $[\text{Co}(\text{CN})_3]^{6-}$  confirmed a  $d^{10}s^0$  closed-shell configuration for cobalt, and significantly reduced cyanide ligands due to Co–C  $\pi$ -bonding and the occupancy of the antibonding CN  $\pi^*$  orbital. The complex is therefore better described as  $[\text{Co}^-(\text{CN}^{1.67-})_3]$ , instead of the purely formal notation  $[\text{Co}^{\text{III}}(\text{CN}^-)_3]^{6-}$ . In this regard, Kaim pointed out the non-innocent nature of  $\text{CN}^-$ .<sup>[5]</sup> Comparable rhodates and iridates reported later displayed similar features.<sup>[6]</sup> This bonding scheme is well-known in carbonyl chemistry containing carbon monoxide isoelectronic to  $\text{CN}^-$ .<sup>[7]</sup> Non-innocent CO ligands are able to stabilize transition metal oxidation states as low as –IV, for example, in  $[\text{Cr}(\text{CO})_4]^{4-}$ , which is the lowest transition metal oxidation state known so far.<sup>[8]</sup>

Our quest for even higher reduced cyanidometalates containing other transition metals led to the ferrates and ruthenates  $\text{LiSr}_3[\text{Fe}(\text{CN})_3]$  and  $\text{AE}_{3.5}[\text{M}(\text{CN})_3]$  ( $\text{AE} = \text{Sr}, \text{Ba}$ ;  $\text{M} = \text{Fe}, \text{Ru}$ ). Their  $[\text{Fe}(\text{CN})_3]^{7-}$  and  $[\text{Ru}(\text{CN})_3]^{7-}$  anions are isoelectronic to  $[\text{Co}(\text{CN})_3]^{6-}$  and feature the extremely rare oxidation state –IV on a transition metal. This is, to the best of our knowledge, the highest negative oxidation state reported for group 8 elements.

[\*] Dr. F. Jach, Dr. F. R. Wagner, Dr. Y. Prots, Dr. M. Bobnar, Prof. Dr. M. Ruck, Dr. P. Höhn  
 Max-Planck-Institute for Chemical Physics of Solids  
 Nöthnitzer Strasse 40, 01187 Dresden (Germany)  
 E-mail: Franziska.Jach@tu-dresden.de  
 Dr. F. Jach, Dr. J. Hunger, Dr. M. Kaiser, Prof. Dr. M. Ruck  
 Faculty of Chemistry and Food Chemistry  
 Technische Universität Dresden  
 01062 Dresden (Germany)  
 Z. H. Amber, Dr. M. Rüsing, Prof. Dr. L. M. Eng  
 Institute of Applied Physics  
 Technische Universität Dresden  
 01062 Dresden (Germany)  
 Dr. M. Bobnar  
 current address: J. Stefan Institute  
 Jamova 39, 1000 Ljubljana (Slovenia)

Dr. A. Jesche  
 Institute of Physics, University of Augsburg  
 Universitätsstrasse 1, 86159 Augsburg (Germany)  
 Prof. Dr. L. M. Eng, Prof. Dr. M. Ruck  
 Würzburg-Dresden Cluster of Excellence ct.qmat  
 Technische Universität Dresden  
 01062 Dresden (Germany)

 Supporting information and the ORCID identification number(s) for the author(s) of this article can be found under:  
 <https://doi.org/10.1002/anie.202103268>.

 © 2021 The Authors. Angewandte Chemie International Edition published by Wiley-VCH GmbH. This is an open access article under the terms of the Creative Commons Attribution Non-Commercial License, which permits use, distribution and reproduction in any medium, provided the original work is properly cited and is not used for commercial purposes.

## Results and Discussion

## Synthesis

Air and moisture sensitive, nearly single-phase microcrystalline powders of  $\text{LiSr}_3[\text{Fe}(\text{CN})_3]$  and  $\text{AE}_{3.5}[\text{M}(\text{CN})_3]$  ( $\text{AE} = \text{Sr}, \text{Ba}$ ;  $\text{M} = \text{Fe}, \text{Ru}$ ) were obtained by reacting pelletized mixtures of alkaline earth subnitrides, transition metals, graphite, and  $\text{Li}_3\text{N}$ ,  $\text{NaCN}$ , or  $\text{NaN}_3$  as additional nitrogen source at 1070 K.  $\text{NaN}_3$  was used instead of gaseous  $\text{N}_2$  to control the nitrogen partial pressure during synthesis. If the nitrogen content is too high, thermodynamically more stable carbodiimides, for example,  $\text{AE}[\text{CN}_2]$  ( $\text{AE} = \text{Ba}, \text{Sr}$ ),<sup>[9]</sup> are formed. Black, needle-shaped single crystals of  $\text{LiSr}_3[\text{Fe}(\text{CN})_3]$  and  $\text{Ba}_{3.5}[\text{Fe}(\text{CN})_3]$  were obtained from a slowly cooled solution of the starting materials in lithium and sodium

flux, respectively. Lithium was removed from the mixture by a modified high-temperature centrifugation-aided filtration,<sup>[10]</sup> sodium was distilled after the reaction.

## Crystal structures

The hexagonal crystal structure of  $\text{LiSr}_3[\text{Fe}(\text{CN})_3]$  ( $P6_3/m$ ) was solved from single-crystal X-ray diffraction data (Figure 1 a,c,e). It is closely related to that of  $\text{Ba}_3[\text{Co}(\text{CN})_3]$ .<sup>[4]</sup> Both contain isoelectronic trigonal planar anions  $[\text{Co}(\text{CN})_3]^{6-}$  and  $[\text{Fe}(\text{CN})_3]^{7-}$ , respectively, which are surrounded by tri-capped trigonal  $\text{AE}_9$ -prisms. Both structures would be isostructural except for one significant difference: the hexagonal channels running along  $[001]$  are empty in  $\text{Ba}_3[\text{Co}(\text{CN})_3]$ , but completely filled with  $\text{Li}^+$  cations in  $\text{LiSr}_3[\text{Fe}(\text{CN})_3]$ .

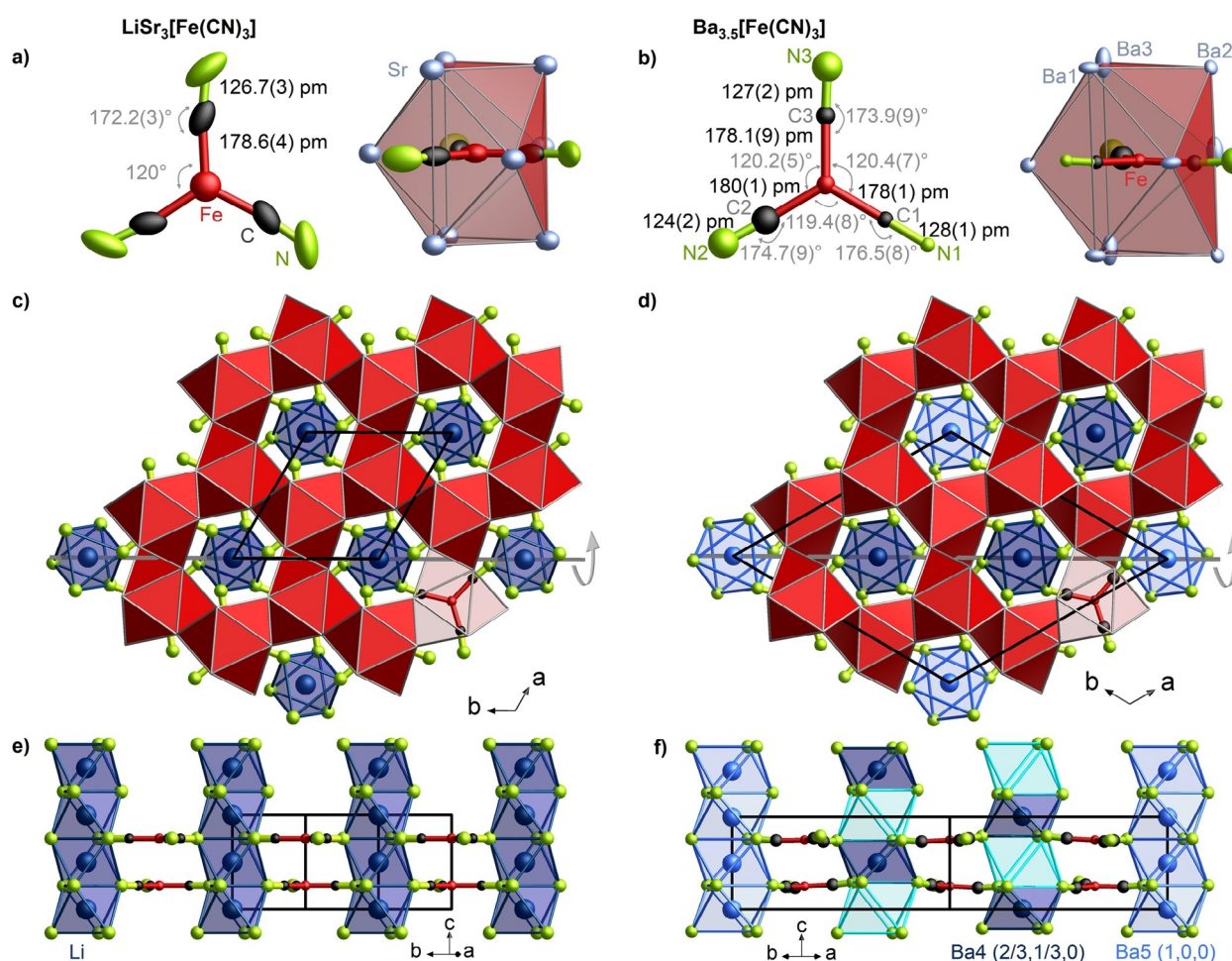


**Figure 1.** Crystal structures of  $\text{LiSr}_3[\text{Fe}(\text{CN})_3]$  ( $P6_3/m$ , no. 176,  $Z=2$ ,  $a=844.07(2)$  pm,  $c=543.30(1)$  pm, 300 K, left) and  $\text{Ba}_{3.5}[\text{Fe}(\text{CN})_3]$  ( $P6_3$ , no. 173,  $Z=6$ ,  $a=1558.78(2)$  pm,  $c=572.27(1)$  pm, 100 K, right). a)  $\text{Li}_3[\text{Fe}(\text{CN})_3]^{7-}$ : trigonal planar anion  $[\text{Fe}(\text{CN})_3]^{7-}$  with bond lengths (black) and angles (gray) as well as strontium environment of  $[\text{Fe}(\text{CN})_3]^{7-}$  in the form of a tri-capped trigonal prism. The ellipsoids comprise 99% probability. b)  $\text{Ba}_{3.5}[\text{Fe}(\text{CN})_3]^{7-}$ : distorted trigonal anion  $[\text{Fe}(\text{CN})_3]^{7-}$  with bond lengths and angles as well as barium environment of  $[\text{Fe}(\text{CN})_3]^{7-}$  in the form of a distorted tri-capped trigonal prism. The ellipsoids comprise 99% probability. c) Honeycomb motif of  $\text{Sr}_9[\text{Fe}(\text{CN})_3]$  prisms (red) in the  $ab$  plane. d) Honeycomb motif of  $\text{Ba}_9[\text{Fe}(\text{CN})_3]$  prisms (red) in the  $ab$  plane. e)  $[\text{LiN}_6]$  octahedra (dark blue), running inside the hexagonal channels along  $[001]$ .  $\text{Li}^+$  is located in between every layer of complex  $[\text{Fe}(\text{CN})_3]^{7-}$  anions.  $\text{Sr}_9[\text{Fe}(\text{CN})_3]$  prisms are omitted in this view for simplicity reasons. Viewed along  $[210]$ . f)  $[\text{BaN}_6]$  octahedra, running inside the hexagonal channels along  $[001]$ . In the central channels (2/3,1/3,z), occupied (Ba4, dark blue) and unoccupied (cyan) octahedra alternate, whereas each octahedron at (0,0,z) is half occupied (Ba5, light blue). That is, half of the octahedral voids are filled with Ba5 atoms indicating a local alternating ordering within each light blue channel.  $\text{Ba}_9[\text{Fe}(\text{CN})_3]$  prisms are omitted in this picture for simplicity reasons, viewed along  $[110]$ .<sup>[13]</sup>

(CN)<sub>3</sub>, providing for the additional negative charge on the cyanidoferrate. Closely related structure types are known for nitridometalates such as Ba<sub>3</sub>[FeN<sub>3</sub>], which contains empty channels,<sup>[11]</sup> and acetylidometalates such as La<sub>3.65</sub>[Ru(C<sub>2</sub>)<sub>3</sub>], which contains La filled channels along [001].<sup>[12]</sup> The lithium environment in LiSr<sub>3</sub>[Fe(CN)<sub>3</sub>] can also be described as chains of face-sharing [LiN<sub>6</sub>] octahedra, using the nitrogen atoms of the CN ligands. In LiSr<sub>3</sub>[Fe(CN)<sub>3</sub>], Li<sup>+</sup> cations center every octahedron in the chain. This structure model yielded good figures of merit and a low residual electron density, but large and unusually oriented displacement ellipsoids especially for the carbon and nitrogen atoms. It looks as if two bonding situations with slightly different bond lengths Fe–C and C–N are superimposed, one of which deviates from linearity. Neither alternative models with lower space group symmetry or the introduction of split atomic positions nor a diffraction experiment at 100 K helped to resolve the situation. Nevertheless, the interatomic distances correspond to the values determined for [Fe(CN)<sub>3</sub>]<sup>7-</sup> in Ba<sub>3.5</sub>[Fe(CN)<sub>3</sub>].<sup>[13]</sup>

The acentric hexagonal crystal structure of Ba<sub>3.5</sub>[Fe(CN)<sub>3</sub>] (P6<sub>3</sub>) may be regarded as an intermediate between the structures of Ba<sub>3</sub>[Co(CN)<sub>3</sub>] and LiSr<sub>3</sub>[Fe(CN)<sub>3</sub>]. The Ba<sub>3.5</sub>[Fe(CN)<sub>3</sub>] (Figure 1b,d,f) crystal structure exhibits a three-fold unit cell in *ab* with respect to the unit cell of LiSr<sub>3</sub>[Fe(CN)<sub>3</sub>] and Ba<sub>3</sub>[Co(CN)<sub>3</sub>] (*a* = 844.07(2) pm for LiSr<sub>3</sub>[Fe(CN)<sub>3</sub>], *a*' = 905.3(1) pm for Ba<sub>3</sub>[Co(CN)<sub>3</sub>],<sup>[4]</sup>  $\sqrt{3}a' \approx a = 1558.78(2)$  pm for Ba<sub>3.5</sub>[Fe(CN)<sub>3</sub>]) as evidenced from superstructure reflections in powder and single-crystal data (Figure S1). The divalent barium atoms alternately occupy half of the octahedra that form the channels along [001]. X-ray diffraction data showed no full long-range ordering, but partial ordering in a superstructure resulting in two distinct kinds of channels: within the two central channels in (1/3, 2/3, *z*) and (2/3, 1/3, *z*), every other octahedron is alternately centered by Ba4 and compressed along [001], whereas the empty octahedra are elongated in this direction (Figure 1f). In contrast, Ba<sup>2+</sup> cations on the half-occupied position Ba5 within the cell-edge channels center every other octahedron of this chain. This is a striking example of geometric frustration, since it is not possible to have a 1:1 alternate ordering of the channels under hexagonal or trigonal symmetry.

Besides the enlarged unit cell, the [Fe(CN)<sub>3</sub>]<sup>7-</sup> anion geometry is likewise affected: In LiSr<sub>3</sub>[Fe(CN)<sub>3</sub>], site symmetry  $\bar{6}$  on Fe yields a planar anion geometry, which is even close to trigonal-planar symmetry *D*<sub>3h</sub> (Figure 1a). In contrast, anion and surrounding prism are distorted in Ba<sub>3.5</sub>[Fe(CN)<sub>3</sub>] (site symmetry 1 on Fe). Despite this low site symmetry, the anion's deviation from trigonal point symmetry *C*<sub>3</sub> is relatively small (Figure 1b).<sup>[13]</sup>

The crystal structures of the isotopic compounds Sr<sub>3.5</sub>[Fe(CN)<sub>3</sub>], Ba<sub>3.5</sub>[Ru(CN)<sub>3</sub>], and Sr<sub>3.5</sub>[Ru(CN)<sub>3</sub>] were refined from synchrotron powder diffraction data and are in good accordance to that of Ba<sub>3.5</sub>[Fe(CN)<sub>3</sub>].<sup>[13]</sup>

## Second-harmonic (SH) microscopy

Confocal second-harmonic (SH) microscopy<sup>[14]</sup> was performed on Ba<sub>3.5</sub>[Fe(CN)<sub>3</sub>] and LiSr<sub>3</sub>[Fe(CN)<sub>3</sub>]. Since second-harmonic generation is only allowed for acentric compounds, a SH response is expected for Ba<sub>3.5</sub>[Fe(CN)<sub>3</sub>], but not for centrosymmetric LiSr<sub>3</sub>[Fe(CN)<sub>3</sub>]. By comparing signals from both compounds, surface effects or other reasons for an SH response can be excluded. For Ba<sub>3.5</sub>[Fe(CN)<sub>3</sub>], SH microscopy images show a SH response over the complete sample area within the glass capillary with individual crystallites visible (Figure 2a). In contrast, most of the image remains dark for LiSr<sub>3</sub>[Fe(CN)<sub>3</sub>] (Figure 2b). The observed weak SHG signal in this picture is strongly localized to a few spots and can be attributed to surface effects. To further evaluate whether the measured signals are due to SH response, the signal intensities were tested as a function of laser power (Figure 2c). For a second harmonic process, the generated signal is expected to scale quadratically with the pump power  $I_{\text{SH}} \propto I_{\text{pump}}^2$ . Albeit observed for both compounds, the quadratic response for Ba<sub>3.5</sub>[Fe(CN)<sub>3</sub>] is 20 times larger as compared to LiSr<sub>3</sub>[Fe(CN)<sub>3</sub>] (Table S10). Due to the random orientation of the

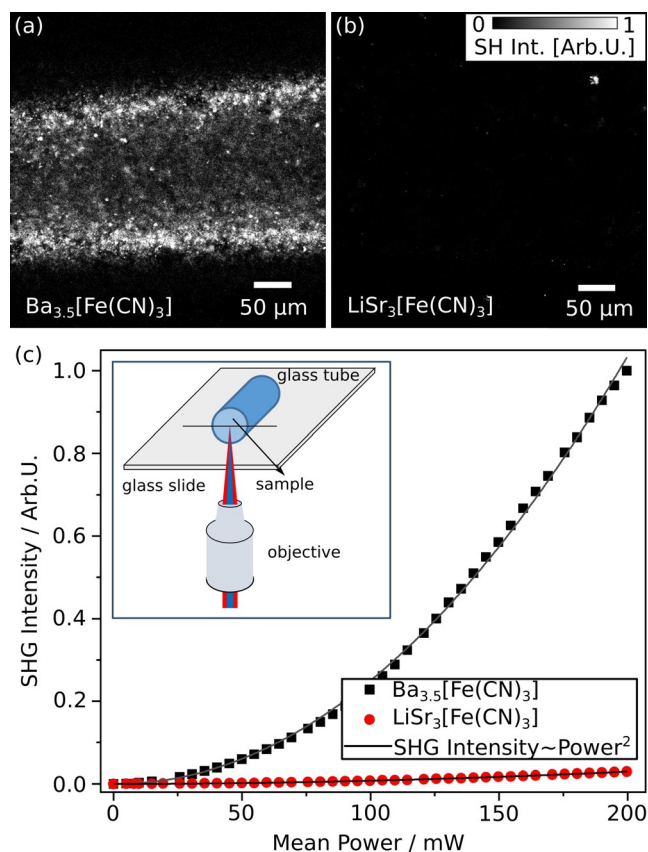


**Figure 2.** Second-harmonic (SH) microscopy images recorded with the same microscope settings (65 mW at 850 nm wavelength) of a) Ba<sub>3.5</sub>[Fe(CN)<sub>3</sub>] and b) LiSr<sub>3</sub>[Fe(CN)<sub>3</sub>] powder samples in glass capillaries. The response appears to be stronger at the glass tube walls due to less scattering and absorption compared to the center. c) A large quadratic dependence of SH intensity on the incident laser power was found for Ba<sub>3.5</sub>[Fe(CN)<sub>3</sub>] compared to LiSr<sub>3</sub>[Fe(CN)<sub>3</sub>]. The resulting data sets were fitted with a quadratic function of the form  $y = ax^b$ .

micro-crystallites we cannot draw any conclusion on the magnitude of individual nonlinear tensor elements (see SI for additional information). Summarizing, the SH analysis corroborates an acentric crystal structure for  $\text{Ba}_{3.5}[\text{Fe}(\text{CN})_3]$ .

### Vibrational spectroscopy

Raman spectra of  $\text{LiSr}_3[\text{Fe}(\text{CN})_3]$  and  $AE_{3.5}[M(\text{CN})_3]$  ( $AE = \text{Sr, Ba}$ ;  $M = \text{Fe, Ru}$ ) exhibit  $\nu(\text{CN})$  valence vibrations clearly distinguishable from bands in the lower wavenumber region which are assigned to valence  $\nu(\text{MC}_3)$  and deformation vibrations  $\delta(\text{MCN})/\delta(\text{CMC})$ , as well as external (lattice) modes (Figure 3, for IR spectra see Figure S7). The vibrational spectra of all compounds are very similar with respect to the number of observed bands in each region; splitting of the  $\nu(\text{CN})$  modes does not occur. This is remarkable with respect to results of molecular site group analysis (Tables S11, S12),<sup>[15]</sup> which yields very different expectations for the nearly trigonal planar anions in  $\text{LiSr}_3[\text{Fe}(\text{CN})_3]$  and the distorted anions in  $AE_{3.5}[M(\text{CN})_3]$ . Considering Raman active  $\nu(\text{CN})$  valence modes as an example, two modes ( $A_g + E_{2g}$ ) are expected for  $\text{LiSr}_3[\text{Fe}(\text{CN})_3]$ , whereas seven Raman active modes ( $3A + 2B + 2E_1 + 2E_2$ ) are expected for  $AE_{3.5}[M(\text{CN})_3]$  because both site symmetry and factor group are lower in the latter case. In contrast, the experimental spectra do not even differ significantly from the expected spectrum of an isolated

**Table 1:** Comparison of cyanide, carbonyl, and acetylide compounds with respect to their bond lengths (pm) and stretching frequencies ( $\text{cm}^{-1}$ ).

Ligand/ Anion	Compound	$d(\text{CN})$	$\nu(\text{CN})$ IR	$\nu(\text{CN})$ Raman	Ref.
CN	$\text{LiSr}_3[\text{Fe}(\text{CN})_3]$	126.7(3)	1490	1581	this work
	$\text{Ba}_{3.5}[\text{Fe}(\text{CN})_3]$	128(1)	1484	1553	this work
		124(2)			
		127(2)			
	$\text{Sr}_{3.5}[\text{Fe}(\text{CN})_3]$	128(4) <sup>[a]</sup>	–	1591	this work
	$\text{Sr}_{3.5}[\text{Ru}(\text{CN})_3]$	126(8) <sup>[a]</sup>	1538	1634	this work
	$\text{Ba}_{3.5}[\text{Ru}(\text{CN})_3]$	124(7) <sup>[a]</sup>	1510	1592	this work
	$\text{Ba}_3[\text{Co}(\text{CN})_3]$	123.5(5)	1680	1696	[4]
	$\text{Na}_2[\text{Cu}(\text{CN})_3] \cdot 3 \text{H}_2\text{O}$	113–116	2090–2110	2090–2122	[17]
	NaCN	116	2088	–	[16]
CO	$\text{Na}_3[\text{Co}(\text{CO})_3]$	126 <sup>[b]</sup>	1614	–	[22]
	$A[\text{Co}(\text{CO})_4]$ ( $A = \text{QuinH, Na}$ ) <sup>[c]</sup>	115	1886	1883–1918	[18, 19]
	$A_2[\text{Fe}(\text{CO})_4]$ ( $A = \text{K, Na}$ )	118	1729–1786	1788	[19, 20]
	$\text{CO}$ (gas)	113	2143	–	[16, 23]
	CC	$\text{La}_{3.65}[\text{Ru}(\text{C}_2)_3]$	130–135	–	–
	$\text{CaC}_2$	120(2)	–	1860	[21]

[a] Averaged distances derived from powder diffraction data. These values are not accurate enough for detailed analysis and are provided for completeness only.<sup>[13]</sup> [b] Calculated values. [c] QuinH = quinuclidinium.

complex anion with trigonal planar point symmetry  $D_{3h}$ . Moreover, the  $\nu(\text{CN})$  stretching frequencies are very similar for  $[\text{Fe}(\text{CN})_3]^{7-}$  and  $[\text{Ru}(\text{CN})_3]^{7-}$  in all examined compounds (Figure 3, Table 1). Thus, the small structural differences do not reflect significant chemical bonding differences for the isoelectronic anions in  $\text{LiSr}_3[\text{Fe}(\text{CN})_3]$  and  $AE_{3.5}[M(\text{CN})_3]$ .

These very electron-rich 18e cyanidoferrates and ruthenates exhibit extremely weakened C–N bonds in comparison to simple cyanide salts (e.g. NaCN) or classical cyanidometalates such as  $[\text{Cu}(\text{CN})_3]^{2-}$  as revealed by elongated distances and reduced stretching frequencies (Table 1).<sup>[16, 17]</sup> Because of the higher anion charge, the effects are even stronger than in the previously reported  $[\text{Co}(\text{CN})_3]^{6-}$ .<sup>[4]</sup> A related frequency decrease of  $\nu(\text{CO})$  was observed for the isoelectronic carbonylmetalates  $[\text{Co}(\text{CO})_4]^-$  and  $[\text{Fe}(\text{CO})_4]^{2-}$ .<sup>[18–20]</sup> Regarding acetylidometalates like  $\text{La}_{3.65}[\text{Ru}(\text{C}_2)_3]$ ,<sup>[12]</sup> a similar weakening of the C–C bonds is observed compared to simple salts like  $\text{CaC}_2$  (Table 1).<sup>[21]</sup> However, quantum chemical calculations confirmed significant La–Ru interactions interlinking the  $[\text{Ru}(\text{C}_2)_3]$  units,<sup>[12]</sup> obscuring the comparison to the cyanidometalates considered here.

### Magnetic properties and electrical conductivity

Magnetic susceptibility measurements on crystals of  $\text{LiSr}_3[\text{Fe}(\text{CN})_3]$  and powder samples of  $\text{Sr}_{3.5}[\text{Ru}(\text{CN})_3]$  revealed diamagnetic behavior (Figure S8a,b). While  $\text{Ba}_{3.5}[\text{Fe}(\text{CN})_3]$  is electrically insulating, semiconducting behavior was observed for  $\text{Sr}_{3.5}[\text{Fe}(\text{CN})_3]$  (Figure S8c). These physical properties are similar to those of the tricyanidocobaltates  $AE_3[\text{Co}(\text{CN})_3]$  ( $AE = \text{Sr, Ba}$ ).<sup>[4]</sup>

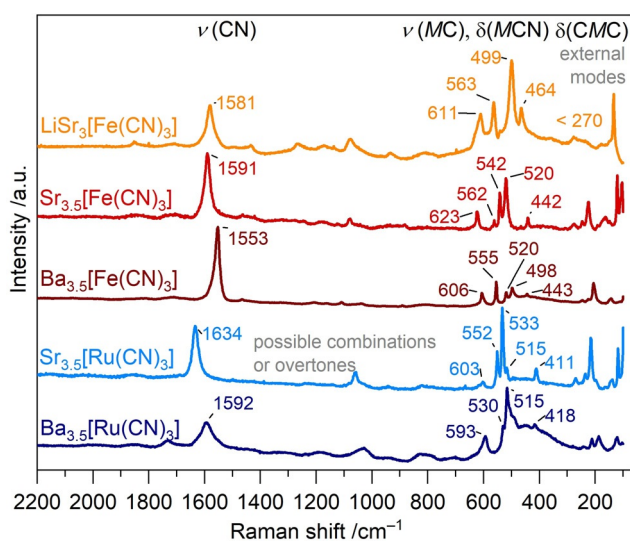


**Figure 3.** Raman spectra of highly reduced cyanidometalates containing  $[\text{Fe}(\text{CN})_3]^{7-}$  and  $[\text{Ru}(\text{CN})_3]^{7-}$  complex anions.

## Quantum chemical calculations

In the following analysis it will be shown that the electronic situation in  $\text{LiSr}_3[\text{Fe}(\text{CN})_3]$  is qualitatively similar to  $\text{Ba}_3[\text{Co}(\text{CN})_3]$ ,<sup>[4]</sup> but features a quantitative difference important for understanding the systematic decrease of the C–N stretching frequency. The naming of the different DOS regions is kept consistent with the one of the previous analysis.<sup>[4]</sup>

As can be seen from Table 2, region A0 corresponds to nominal Sr(4p<sup>6</sup>) semicore states, regions A1, A2, and B to the nominal states of a CN<sup>1-</sup> ligand, and a region C = C1 + C2 to the states of a formal Fe(3d<sup>10</sup>) species. The significant contributions of the CN ligand to the nominal Fe(3d) regions is characteristic for the actual covalency Fe–C and the Fe → C–N  $\pi$  backbonding mechanism leading to a C–N bond weakening as described in the Dewar-Chat-Duncanson model.<sup>[7]</sup> Similar to  $AE_3[\text{Co}(\text{CN})_3]$  ( $AE = \text{Sr}, \text{Ba}$ ) reported earlier,<sup>[4]</sup> also in isoelectronic  $\text{LiSr}_3[\text{Fe}(\text{CN})_3]$  there is an additional C–N  $\pi$  antibonding state D occupied with two electrons per formula unit. But unlike to the previous Co case, it overlaps with the top of the nominal Fe(3d<sup>10</sup>) valence bands, i.e., with region C2 containing the Fe(3d<sub>2</sub>) contributions (Figure 4a, inset). For this reason, a plot of the electron density of only the higher energy part of DOS peak D with 1.74 e/f.u. omitting the Fe(3d<sub>2</sub>) local DOS peak is shown in Figure 4b. The C–N  $\pi$  antibonding characteristic is clearly visible. The integrated values for DOS region D (Table 2) were obtained including the overlapping region with C2 (see Figure 4a, inset) in order to maintain the ideal electron count of 2 e/f.u. This results in a certain overestimation of the Fe contributions for region D, but it does not affect the total electronic populations and effective charges  $Q^{\text{eff}}$  of the QTAIM atoms. Since the CN group still turns out to be the main contributor of this DOS region, the major conclusion is left unaffected, namely, that the complete DOS region D with 2 e/f.u. is to be formally attributed to three CN ligands per formula unit. In connection with DOS regions A1, A2, and B the final formal charge attribution yields  $(\text{CN})^{1.67-}$ , similar to  $\text{Ba}_3[\text{Co}(\text{CN})_3]$ .<sup>[4]</sup> However, as a quantitative difference to  $\text{Ba}_3[\text{Co}(\text{CN})_3]$ , it is to be noted that the CN group effective charge of 1.66– in the Fe compound turns out to be higher than 1.39– obtained for the Co compound. This difference of 0.27 electrons is mainly caused by regions C and D, where the Fe compound exhibits 0.21 electrons more on the CN groups

**Table 2:** QTAIM atomic site projection of DOS regions A0 to D. The portion of electrons of each QTAIM atomic species per formula unit is given in percent of the nominal electron count for each DOS region. The resulting QTAIM effective charges  $Q^{\text{eff}}$  are given at the bottom of the table.

	Nom. e/f.u.	1 Li	3 Sr	1 Fe	3 CN
DOS A0	18	0.0	89.8	0.3	9.9
DOS A1	6	0.0	20.5	0.2	79.2
DOS A2	6	0.4	3.6	8.3	87.6
DOS B	18	0.3	5.9	7.2	86.6
DOS C (1 + 2)	10 (8 + 2)	0.3	8.0	55.4	36.2
DOS D	2	0.4	18.8	32.3	48.5
$Q^{\text{eff}}$		$\text{Li}^{0.88+}$	$\text{Sr}^{1.38+}$	$\text{Fe}^{0.04-}$	$\text{CN}^{1.66-}$

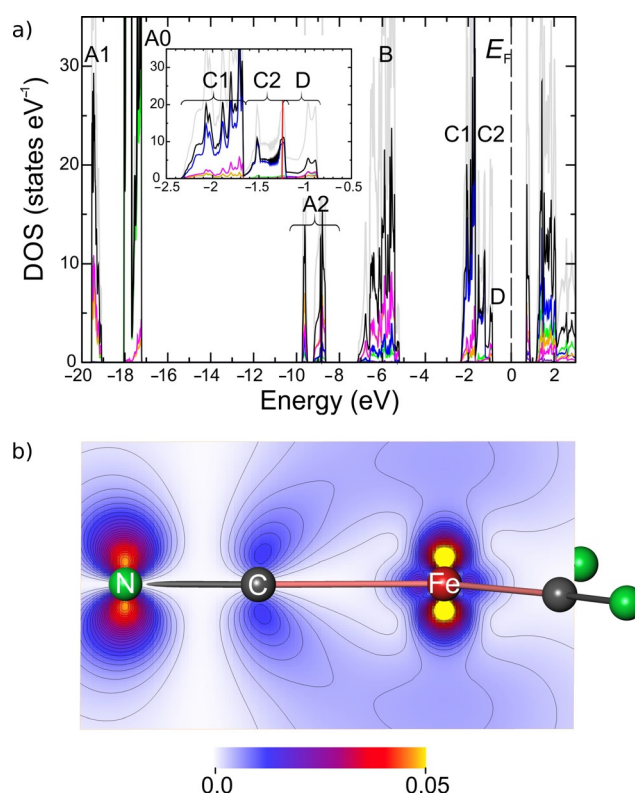


**Figure 4.** a) DOS for  $\text{LiSr}_3[\text{Fe}(\text{CN})_3]$  (total DOS gray, muffin-tin part black, Li partial DOS (pDOS) cyan, Sr pDOS green, Fe pDOS blue, C orange, and N magenta). Inset shows detailed view on DOS regions C (composed of C1 and C2) and D indicating slight overlap between C2 and D, where vertical red line marks boundary between nominal C1 + C2 (10 e/f.u.) and D (4 e/f.u.) regions. b) Electron density calculated for electronic states from upper part of DOS region D with 1.74 e/f.u. See text for further details.

than the Co compound. Since regions C and D are characterized by C–N  $\pi$  antibonding orbitals, the Fe compound with its higher populated C–N antibonding bands is expected to display weaker C–N bonds, which is corroborated by the trend observed for the C–N stretching frequencies. Summarizing, the nominal d<sup>10</sup>s<sup>0</sup> Fe<sup>2+</sup> compound features a lower effective electron count on the transition metal than the nominally isoelectronic Co<sup>1+</sup> compound, which yields a reverse behavior for the effective electron counts of the nominally isoelectronic CN ligands. Thus, for this scenario, the compound with the more negative transition metal oxidation state is expected to display the weaker C–N bonds.

## Conclusion

The herein reported cyanidometalates  $\text{LiSr}_3[\text{Fe}(\text{CN})_3]$  and  $AE_{3,5}[M(\text{CN})_3]$  ( $AE = \text{Sr}, \text{Ba}; M = \text{Fe}, \text{Ru}$ ) adopt a very versatile structure type, which is also known for isoelectronic cyanidometalates  $\text{Ba}_3[M(\text{CN})_3]$  ( $M = \text{Co}, \text{Rh}, \text{Ir}$ ), nitridometalates (e.g.  $\text{Ba}_3[\text{FeN}_3]$ ),<sup>[6]</sup> and acetylidometalates (e.g.  $\text{La}_{3,65}[\text{Ru}(\text{C}_2)_3]$ ).<sup>[12]</sup> A common feature of all these metalates is the tricapped trigonal prismatic environment of alkaline earth or rare earth cations, which apparently provides a stable

host for the highly charged trigonal planar anions. Channels in the structure allow further stabilization, for example, by additional charge balance in case of  $\text{Li}^+$  or  $\text{AE}^{2+}$  filled channels in  $\text{LiSr}_3[\text{Fe}(\text{CN})_3]$  and  $\text{AE}_{3.5}[\text{M}(\text{CN})_3]$  ( $\text{AE} = \text{Sr}, \text{Ba}; \text{M} = \text{Fe}, \text{Ru}$ ), or by Ru–La interactions in  $\text{La}_{3.65}[\text{Ru}(\text{C}_2)_3]$ .<sup>[12]</sup> Hence, varying the components of this structure type, such as complex anions, prism cations, and channel atoms, allows the fine-tuning of the electronic structure and therefore of the physical properties. The mutual bonding scheme of the highly reduced 18e cyanidometalates  $[\text{Co}(\text{CN})_3]^{6-}$ ,  $[\text{Fe}(\text{CN})_3]^{7-}$ , and  $[\text{Ru}(\text{CN})_3]^{7-}$  includes a closed-shell metal  $d^{10}s^0$  configuration and significantly reduced, non-innocent  $\text{CN}^{1.67-}$  ligands, as in  $[\text{Fe}^{2-}(\text{CN}^{1.67-})_3]$ . The higher the charge on the metalate, the weaker the C–N bonds, resulting in extremely low  $\nu(\text{CN})$  vibration frequencies for the  $[\text{M}(\text{CN})_3]^{7-}$  anions. The new ferrates and ruthenates are not only unprecedented with respect to cyanidometalates: An analogous carbonylmetalate  $[\text{Fe}(\text{CO})_3]^{4-}$  remains unknown, and  $[\text{Fe}(\text{CN})_3]^{7-}$  and  $[\text{Ru}(\text{CN})_3]^{7-}$  represent the first examples of group 8 elements with an oxidation state of –IV. It seems, that the “adventures with substances containing metals in negative oxidation states” (Ellis)<sup>[24]</sup> will continue with the growing class of highly reduced cyanidometalates.

## Acknowledgements

We gratefully acknowledge Dr. H. Borrmann and S. Hückmann for X-ray powder diffraction data collection, K. Zechel and G. Yildirim for help with sample preparation, Dr. W. Schnelle and R. Koban for physical property measurements, as well as U. Schmidt and A. Völzke for chemical analyses. We are thankful to Prof. Dr. J. J. Weigand, TU Dresden, for the opportunity to use the SuperNova single crystal diffractometer. We acknowledge the European Synchrotron Radiation Facility for provision of synchrotron radiation facilities, and we would like to thank Dr. A. Fitch for assistance in using beamline ID22. This work was supported by the Light Microscopy Facility, a Core Facility of the CMCB Technology Platform at TU Dresden. We thank the German Research Foundation (DFG) for financial support (project-id 422042965). Open access funding enabled and organized by Projekt DEAL.

## Conflict of interest

The authors declare no conflict of interest.

**Keywords:** electronic structure · non-innocent ligand · Raman spectroscopy · second harmonic generation · solid-state structures

[1] A. Kraft, *Nachr. Chem.* **2010**, *58*, 1124–1127; and references therein.

[2] C. K. Jørgensen, *Oxidation Numbers and Oxidation States*, Springer, Heidelberg, **1969**.

- [3] a) A. G. Sharpe, *The Chemistry of Cyano Complexes of Transition Metals*, Academic Press, London, **1976**; b) K. R. Dunbar, R. A. Heintz, *Prog. Inorg. Chem.* **1997**, *45*, 283–391.
- [4] P. Höhn, F. Jach, B. Karabiyik, Yu. Prots, S. Agrestini, F. R. Wagner, M. Ruck, L. H. Tjeng, R. Kniep, *Angew. Chem. Int. Ed.* **2011**, *50*, 9361–9364; *Angew. Chem.* **2011**, *123*, 9533–9536.
- [5] W. Kaim, *Angew. Chem. Int. Ed.* **2011**, *50*, 10498–10500; *Angew. Chem.* **2011**, *123*, 10682–10684.
- [6] a) F. Jach, P. Höhn, Yu. Prots, M. Ruck, *Z. Anorg. Allg. Chem.* **2015**, *641*, 998–1001; b) F. Jach, P. Höhn, A. Senyshyn, M. Ruck, R. Kniep, *Z. Anorg. Allg. Chem.* **2012**, *638*, 1959–1961.
- [7] C. Janiak, T. M. Klapötke, H.-J. Meyer, *Moderne Anorganische Chemie*, 2nd ed. (Ed. E. Riedel), de Gruyter, Berlin, **2003**.
- [8] J. T. Lin, G. P. Hagen, J. E. Ellis, *J. Am. Chem. Soc.* **1983**, *105*, 2296–2303.
- [9] U. Berger, W. Schnick, *J. Alloys Compd.* **1994**, *206*, 179–184.
- [10] a) M. Boström, S. Hovmöller, *J. Alloys Compd.* **2001**, *314*, 154–159; b) A. Jesche, P. Canfield, *Philos. Mag.* **2014**, *94*, 2372–2402; c) A. Jesche, R. W. McCallum, S. Thimmaiah, J. L. Jacobs, V. Taufour, A. Kreyssig, R. S. Houk, S. L. Bud'ko, P. C. Canfield, *Nat. Commun.* **2014**, *5*, 3333; d) P. Höhn, T. J. Ballé, M. Fix, Yu. Prots, A. Jesche, *Inorganics* **2016**, *4*, 42.
- [11] P. Höhn, R. Kniep, A. Rabenau, *Z. Kristallogr.* **1991**, *196*, 153–158.
- [12] B. Davaasuren, E. Dashjav, T. Doert, G. Kreiner, W. Schnelle, F. R. Wagner, M. Mihalkovič, R. Kniep, *Z. Anorg. Allg. Chem.* **2010**, *636*, 41–49.
- [13] Deposition numbers 2067882 ( $\text{LiSr}_3[\text{Fe}(\text{CN})_3]$ ), 2068069 ( $\text{Ba}_3[\text{Fe}(\text{CN})_3]$ ), 2068088 ( $\text{Sr}_{3.5}[\text{Fe}(\text{CN})_3]$ ), 2068090 ( $\text{Ba}_3[\text{Ru}(\text{CN})_3]$ ) and 2067884 ( $\text{Sr}_{3.5}[\text{Ru}(\text{CN})_3]$ ) contain the supplementary crystallographic data for this paper. These data are provided free of charge by the joint Cambridge Crystallographic Data Centre and Fachinformationszentrum Karlsruhe Access Structures service. For additional details see supporting information Figure S1–S4, Figure S6, and Tables S1–S9.
- [14] a) D. Tan, B. Kirbus, M. Rüsing, T. Pietsch, M. Ruck, L. M. Eng, *Small* **2020**, *16*, 2000857; b) D. Tan, B. Kirbus, L. M. Eng, M. Ruck, *Eur. J. Inorg. Chem.* **2020**, 2465–2469; c) Y. Sheng, A. Best, H. J. Butt, W. Krolkowski, A. Arie, K. Koynov, *Opt. Express* **2010**, *18*, 16539–16545; d) T. Kämpfe, P. Reichenbach, M. Schröder, A. Haußmann, L. M. Eng, T. Woike, E. Soergel, *Phys. Rev. B* **2014**, *89*, 035314; e) T. Kämpfe, P. Reichenbach, A. Haußmann, T. Woike, E. Soergel, L. M. Eng, *Appl. Phys. Lett.* **2015**, *107*, 152905; f) L. Wehmeier, T. Kämpfe, A. Haußmann, L. M. Eng, *Phys. Status Solidi RRL* **2017**, *11*, 1700267; g) O. Sánchez-Dena, E. V. García-Ramírez, C. D. Fierro-Ruiz, E. Viguera-Santiago, R. Farías, J. A. Reyes-Esqueda, *Mater. Res. Express* **2017**, *4*, 035022.
- [15] a) J. Weidlein, U. Müller, K. Dehnicke, *Schwingungsspektroskopie*, Thieme, Stuttgart, **1988**; b) D. L. Rousseau, R. P. Bauman, S. P. S. Porto, *J. Raman Spectrosc.* **1981**, *10*, 253–290.
- [16] A. Hollemann, E. Wiberg, *Lehrbuch der Anorganischen Chemie*, de Gruyter, Berlin, **1995**.
- [17] C. Kappenstein, R. P. Hugel, *Inorg. Chem.* **1978**, *17*, 1945–1949.
- [18] L. Brammer, J. C. Mareque Rivas, D. Zhao, *Inorg. Chem.* **1998**, *37*, 5512–5518.
- [19] a) W. F. Edgell, J. Huff, J. Thomas, H. Lehman, C. Angell, G. Asato, *J. Am. Chem. Soc.* **1960**, *82*, 1254–1255; b) H. Stammreich, K. Kawai, Y. Tavares, P. Krumholz, J. Behmoiras, S. Bril, *J. Chem. Phys.* **1960**, *32*, 1482–1487.
- [20] a) R. G. Teller, R. G. Finke, J. P. Collman, H. B. Chin, R. Bau, *J. Am. Chem. Soc.* **1977**, *99*, 1104–1111; b) J. E. Ellis, *Adv. Organomet. Chem.* **1990**, *31*, 1–51.
- [21] O. Reckweg, A. Baumann, H. A. Mayer, J. Glaser, H.-J. Meyer, *Z. Anorg. Allg. Chem.* **1999**, *625*, 1686–1692.
- [22] a) J. E. Ellis, P. T. Barger, M. L. Winzenburg, G. F. Warnock, *J. Organomet. Chem.* **1990**, *383*, 521–530; b) Z. Chen, Y. Deng, J.

- Bian, L. Li, G. Xu, *J. Mol. Struct.: THEOCHEM* **1998**, *434*, 155–161.
- [23] D. H. Rank, D. P. Eastman, B. S. Rao, T. A. Wiggins, *J. Opt. Soc. Am.* **1961**, *51*, 929–936.
- [24] J. E. Ellis, *Inorg. Chem.* **2006**, *45*, 3167–3186.

Manuscript received: March 5, 2021  
Revised manuscript received: April 27, 2021  
Accepted manuscript online: May 3, 2021  
Version of record online: June 15, 2021

---